Peer-reviewed version available at *Biomolecules* **2019**, *9*, 123; doi:10.3390/biom9040123

Evaluation of anticancer efficacy of cyclosaplin using a Silk based 3D tumor model

Abheepsa Mishra*, Sourav K Mukhopadhyay, Satyahari Dey

Plant Biotechnology Laboratory, Department of Biotechnology, Indian Institute of Technology Kharagpur, Kharagpur-721302, West Bengal, India

Abheepsa Mishra, Ph.D.
Plant Biotechnology Laboratory
Department of Biotechnology
Indian Institute of Technology Kharagpur
Kharagpur-721302, West Bengal, India
E-mail id: abhipsa05@gmail.com

Sourav K Mukhopadhyay, Ph.D.
Plant Biotechnology Laboratory
Department of Biotechnology
Indian Institute of Technology Kharagpur
Kharagpur-721302, West Bengal, India
E-mail id: mukherjeesour@gmail.com

Dr. Satyahari Dey
Plant Biotechnology Laboratory
Department of Biotechnology
Indian Institute of Technology Kharagpur
Kharagpur-721302, West Bengal, India
E-mail id: sdey12.iitkgp@gmail.com

**Corresponding author/Present address*: Dr. Abheepsa Mishra, Postdoctoral Researcher, Department of Internal Medicine, The University of Texas Southwestern Medical Center, 5323 Harry Hines Blvd, Dallas, TX 75390, USA. (T) +1 (518) 881-9196
E-mail address: abhipsa05@gmail.com, abheepsa.mishra@utsouthwestern.edu

Peer-reviewed version available at *Biomolecules* **2019**, *9*, 123; doi:10.3390/biom9040123

Abstract

Development of novel anti-cancer peptides requires a rapid screening process which can be accelerated by using appropriate in vitro tumor models. Breast carcinoma tissue is a three dimensional (3D) microenvironment, which contains a hypoxic center surrounded by dense proliferative tissue. Biochemical clues provided by such 3D cell mass cannot be recapitulated in conventional 2D culture systems. In this experiment, we evaluate the efficacy of the sandalwood peptide, cyclosaplin on established *in vitro* 3D silk breast cancer model using invasive MDA-MB-231 cell line. The anti-proliferative effect of the peptide on 3D silk tumor model is monitored by alamar blue assay, with conventional 2D culture as control. The proliferation rate, glucose consumed, LDH, and MMP-9 activity of Human breast cancer cells are higher in 3D constructs compared to 2D. A higher concentration of drug is required to achieve 50% cell death in 3D culture than 2D cultures. The cyclosaplin treated MDA-MB-231 cells showed significant decrease in MMP-9 activity in 3D constructs. Microscopic analysis revealed the formation of cell clusters evenly distributed in the scaffolds. The drug treated cells were less in number, smaller and showed unusual morphology. Overall, these findings indicate the role of cyclosaplin as a promising anti-cancer therapeutics.

Keywords: Breast cancer; Cyclosaplin; 3D tumor model; Peptide, Sandalwood; Silk

1. Introduction

Three-dimensional (3D) *in vitro* models are currently inevitable in cancer biology as a bridge connecting two-dimensional cultures (2D) and the complexity associated with *in vivo* models. The war against cancer has gained momentum, as it is one of the major causes of death in the world and its story is yet to unfurl. The 2D cell cultures fail to furnish an ideal environment for screening novel anticancer compounds. This leads to the low predictability of these 2D models in preclinical trials [1]. Initially, the traditional spotlight for development of chemotherapeutics was on tumor cells only. Lack of clinical efficacy and unacceptable toxicity are two of the main causes of failures during drug development [2]. The experimental studies revealed that synergy with the stroma in 3D systems might have an impact on sensitivity and resistance to drugs [3]. This highlights the importance of microenvironment in designing and screening the efficacy of new anticancer drugs. The 3D cell culture experiments serve as a convenient platform for probing the above processes [4, 5]. The extracellular matrix (ECM), considered as an essential component of the stroma was shown to stimulate signal transduction pathways that might be absent when the drugs were screened in 2D flasks, devising this approach ineffective on tumors [6]. This could lead to failure in the clinical trials. An *in vitro* tumor model is a vital tool for evaluating therapeutic efficacy of drug before performing *in vivo* experiments. The advancement of translatable drug delivery systems clinically requires intensive evaluation of their tumor targeting potential *in vitro*, therapeutic efficiency, cytotoxic nature, and biocompatibility [7]. Thus to imitate the *in vivo* characteristics of cancerous human tissue and testing the efficacy of anticancer drugs, a 3D model needs to be used. Tumor cell metabolism is one of the important attributes of cancer biology and recently, it has attained new heights. The cancer cells metabolism is altered compared to normal cells and this offers an edge for their survival and growth [8]. In cancer, the metabolism preferably shifts towards glycolytic pathway (glucose to lactate) with a

decreased dependency for oxidative pathway (pyruvate to lactate to acetyl-CoA) [8, 9]. This phenomenon is also known as "Warburg effect". Several factors are involved in cancer pathogenesis, out of which matrix metalloproteinase's (MMPs) are extensively studied. MMPs expression has been found to be upregulated practically in all types of advanced stage cancer in humans with invasive and metastatic potential and poor prognosis [10-12]. Among various MMPs, MMP-9 is the major enzyme for degradation of type IV collagen, a main component of the ECM. It also plays a vital role in tumor angiogenesis by enhancing the VEGF production [13]. Therefore, there is a growing interest in developing 3D *in vitro* models for testing the efficacy of anticancer drugs. Both natural and synthetic matrices have been developed for culture of cancer cells [14].

Silk, a natural polymer is used as multifaceted biomaterial in various form such as films, membranes, gels, sponges, powders, scaffolds [15], and nanoparticles [16, 17]. The proliferation of human MDA-MB-231 cells on silk fibroin 3D model has been reported recently [18]. The 3D silk fibroin model was used to study the efficacy of a few anticancer drugs such as ZD6474, celexocib, and paclitaxel [19]. Our previous work identified and structurally characterized a new cyclic octapeptide cyclosaplin from somatic seedlings of Santalum album L. [20] and to further assess the efficacy of cyclosaplin we employed 3D-based silk tumor models. There are no reports of this silk fibroin models being used to screen new peptide based anticancer agents against breast cancer. In this study, silk fibroin based 3D *in vitro* tumor model was used for evaluating the anticancer efficacy of novel cyclic peptide cyclosaplin and doxorubicin.

2. Materials and methods

2.1 Materials

Alamar blue (Molecular Probes, Invitrogen, USA), cellulose dialysis tubing of cut off 12,000 (Pierce, USA), Dulbecco's Modified Eagle's Medium (DMEM) (Gibco, Invitrogen, USA),

penicillin/streptomycin (Himedia, India), fetal bovine serum (Gibco, Invitrogen, USA), Gelatin (Sigma-Aldrich, USA), Glucose Assay and Lactate assay Kit (Span Diagnostics, India), Live-Dead assay kit (Molecular Probes, Invitrogen, USA), MTT (Himedia, India), Sodium dodecyl sulfate (Pierce, USA), tissue culture grade polystyrene flasks and cell culture plates (Tarsons, India), trypsin-EDTA (Himedia, India).

2.2 Preparation of Fibroin from *A.mylitta* Silkworm

Antheraea mylitta (A.mylitta) silk fibroin was fabricated as described in the earlier reports [18, 21]. The fifth instar mature larvae of *Antheraea mylitta* were dissected to collect the posterior glands. The glands were repeatedly rinsed in distilled water for removing the traces of sericin and squeezed to obtain fibroin protein. The fibroin protein was dissolved in 1% (w/v) SDS aqueous solution comprising 10 mM Tris (pH 8.0) and 5 mM EDTA at room temperature [18]. The solubilized protein was dialyzed (MWCO 12000) against deionized water for regeneration of the 2 % (w/v) aqueous protein solution. The fibroin solution was passed through 0.22 µm filter before casting into moulds for matrix fabrication.

2.3 Fabrication of 2D and 3D silk matrices

The silk fibroin (2% w/v) isolated from *A.mylitta* was used to coat the wells of 96 well tissue culture plates (TCP). The plates were kept overnight for drying, and the films were washed with 70% ethanol followed by PBS. The films were sterilized for 20 mins by UV-treatment. The silk fibroin film-coated tissue culture plates were used in cell culture experiments. For 3D matrices, the silk fibroin solution was pour into plates, freeze at -20^{o}C for 8 h and lyophilized resulting in porous silk fibroin scaffolds [21]. Both the 2D and 3D silk matrices were stabilized by β-sheet formation induced by brief alcohol (absolute ethanol) treatment. The silk fibroin 3D scaffolds were washed in PBS and UV sterilized prior to cell culture studies.

2.4 Culture, maintenance and seeding of MDA-MB-231 cells

MDA MB 231 cells were sub-cultured in Dulbecco's Modified Eagle's Medium (DMEM) containing 10% fetal bovine serum and 1 % penicillin G-streptomycin at 37 °C in 5% CO_2 humidified environment. At confluence, the cells were treated with Trypsin/EDTA to get into suspension, pellet and finally re-suspended in fresh medium for cell seeding. Before cell culture, the silk fibroin matrices were sterilized by consecutive treatment with 70% ethanol and UV light for 30 min. Silk constructs were then washed thrice with sterile PBS (pH 7.4) and conditioned with complete medium for 4 h. Just before cell seeding, the matrices were partially dehydrated for 2 h to ensure proper cell permeability. Approximately 1×10^5 cells were loaded on the silk constructs and left undisturbed in a humidified incubator (37C °C, 5% CO_2) for 30 min for cellular adhesion. The cell laden matrices were then incubated in complete DMEM for 7 days prior to treatment with experimental drugs. The culture medium was replenished after every 2 days.

2.5 Cell proliferation assay

The cell proliferation assay was done by seeding cells on both the 2D (1×10^3) and 3D (1×10^5) silk constructs. Alamar blue, a non-toxic chemical, was used to visualize the reducing environment of the proliferating cell. This assay was executed after 1, 4, and 7 days to confirm cell viability and proliferation of the cells on 2D and 3D constructs [22].

2.6 Chemotherapeutic studies

The human breast cancer cells (MDA-MB-231) were seeded on 2D (1×10^3) and 3D (1×10^5) culture systems separately. The cells were then incubated for 7 days in a CO_2 (5%) chamber at 37 ° C. The cell laden 2D and 3D constructs after 7 days of culture were treated with test compounds for 48 hrs before evaluating for cytotoxic effects by MTT assay. The cells were serum starved for 24 h before drug treatment. The established chemotherapeutic agent doxorubicin served as a positive control for the study. The IC_{50} of cyclosaplin and

doxorubicin were computed for the cells grown in both 2D and 3D constructs. Doxorubicin is used as positive control that interacts with DNA by intercalation, inhibits macromolecular biosynthesis and used for treating breast cancers [23, 24].

2.7 Glucose consumption and Lactic acid production assay

The glucose present in the spent media was determined using the Glucose Assay Kit (Span Diagnostics, India). Briefly, 2µl of spent media was added to 200 µl of enzyme mixture and incubated at 37°C for 30 min. The reaction mixture was well mixed and the absorbance was read at 505 nm using a microplate reader. All the recordings were performed in triplicates. The glucose concentration was analyzed using triplicates of a single standard (1 mg/ml) according to manufacturer's instructions. The amount of glucose consumption was calculated by subtraction of the total glucose present in the media with the glucose left on day 1, 4 or 7 after seeding [18].

$$\text{Glucose} + O_2 + H_2O \xrightarrow{\text{Glucose Oxidase}} \text{Gluconic acid} + H_2O_2$$

$$H_2O_2 + \text{Phenol} + \text{4-AAP} \xrightarrow{\text{Peroxidase}} \text{Quinoneimine dye} + H_2O$$

The lactate present in the spent media was determined using lactate assay kit (Span Diagnostics, India) of grown cells for 1, 4, or 7 days. The cells were incubated at 37°C for 3 min in the dark and then absorbance was read at 340 nm.

$$\text{Pyurvate} + \text{NADH} + H^+ \longrightarrow \text{Lactate} + NAD^+$$

2.8 MMP-9 activity of MDA-MB-231 cells on silk constructs

MMP-9 activity in 2D and 3D silk constructs was analyzed using SDS-PAGE gelatin zymography. MMP-9 activity present in conditioned media was visualized by gelatin zymography as described by Kleiner and Stevenson, 1994. Gels for zymography comprised of 0.1% gelatin and 10% polyacrylamide. Samples were mixed with a Tris-HCl 0.25 M, pH

6.8, SDS 2%, sucrose 4%, bromophenol blue 0.1% buffer and electrophoresed without boiling. For qualitative analysis of gelatinase activities 20 µg of protein from each sample were loaded on to gel. Then gels were incubated in 2.5% Triton X-100 with gentle shaking for 30 min at 20°C. The gels were then incubated for 18 h at 37 °C in substrate buffer (50 mM Tris–HCl, pH 7.6, 200 mM NaCl, 10 mM $CaCl_2$). The gels were stained in 0.5% coomassie blue G-250 in acetic acid/methanol/water (1:4:5) for 30 min after incubation followed by destaining in acetic acid/methanol/water (1:2:7). The proteolytic activities were visualized as clear white zones, demonstrating gelatin degradation in the gels, against the stained blue background. Collagenase (Sigma, USA) was used as a positive control. The MMP-9 activity was analyzed according to its molecular weight (MMP-9: 92 kDa).

2.9 Scanning electron microscopy

MDA-MB-231 cells (1×10^5) were seeded on 3D silk constructs. The 7^{th} day constructs were rinsed in 500 µl of serum-free medium and fixed in 4% paraformaldehyde for 15 min. The samples were washed twice with PBS (pH 7.4), subjected to dehydration using series of 50-100% ethanol (20 min) and vacuum-dried. For SEM, the images were taken after the samples were sputter coated with gold using a JEOL JSM-5800 scanning electron microscope [18, 20].

2.10 Live-dead assay

MDA-MB-231 cells (1×10^5) were seeded on 3D silk fibroin constructs. The viability of MDA-MB-231 cells was measured using a Live-dead viability kit (Invitrogen, USA) following the manufacturer's instruction. The cultures were incubated for in a humidified CO_2 chamber for 7 days at 37°C. The cyclosaplin and doxorubicin induced (1 µg/mL, 100 µg/mL) cells loaded silk constructs were stained with 150 µl live–dead assay reagent (2 µM Calcein AM and 4 µM EthD-1) for 30 min at 25 °C. It was then washed twice in PBS and

visualized under confocal microscope (CLSM; Olympus FV 1000 attached with an inverted microscope IX 81, Japan).

2.11 Analysis of cytoskeletal organization

MDA-MB-231 cells were cultured on 2D (1×10^3) silk constructs as described by Corada et al., 1999. The cells were treated with cyclosaplin and doxorubicin respectively. The 2% paraformaldehyde fixed cells were incubated for 15 min at room temperature followed by permeabilization with 0.5% Triton X-100 before staining. After incubation with the TRITC conjugated phalloidin (1:200 dilution) for 1 h at room temperature followed by rinse with 1x PBS (pH 7.4) counter staining of nucleus was done with Hoeschst (1:1000 dilution) for 15 min at RT. Imaging was done using confocal microscope (CLSM; Olympus FV 1000 attached with an inverted microscope IX 81, Japan).

2.12 Statistical analysis

All the data represents the mean and standard deviation of three samples. Analysis was performed using Student's t-test Graphpad Software QuickCalcs and the significance level of $P < 0.05$ and $P < 0.01$ was employed.

3. Results

3.1 Preparation and fabrication of 2D/3D silk constructs

The fabricated silk constructs without the cells were observed under scanning electron microscope. The 3D silk fibroin scaffolds with interconnected pores are shown in Fig. 1. MDA-MB-231 cells propagated well on 2D fibroin coated plates within 7 days of culture period. In 3D silk constructs, the MDA-MB-231 cells proliferated well, utilizing all the pores of 3D constructs forming clusters.

3.2 Cell Proliferation assay

The proliferation of the invasive breast cancer cells (MDA-MB-231) on 2D and 3D constructs (Fig. 2) were evaluated by alamar blue assay. The cells were proliferative over

time in 3D matrices, while the peak of cell growth in 2D was revealed on 4th day (115.2 ± 1.35 %) followed by a reduction in proliferation rate. The cells in 2D have limited surface area, therefore after a certain confluence level, the viability of cells decreases due to restriction in space to multiply further. The proliferation of cells in 3D, increased over time and is higher than 2D on 7th day (96.22 ± 0.40).

3.3 Chemotherapeutic studies

The MDA-MB-231 cells were cultured for 7 days on *A.myliita* silk constructs *in vitro*, subjected to cyclosaplin and doxorubicin treatment for 48 hrs. The cell viability was studied for various drug concentrations (1-1000 µg/mL) of the peptide (Fig. 3a) and doxorubicin (Fig. 3b). In 2D culture, the IC_{50} concentration for doxorubicin was 2.8 ±.06 µg/mL, whereas the IC_{50} of cyclosaplin was 16.86±0.09 µg/mL. In 3D culture, the IC_{50} concentration for doxorubicin was 16.44±0.1 µg/mL, while the IC_{50} of cyclosaplin was 89.27 ± 0.2 µg/mL. The higher concentrations of cyclosaplin and doxorubicin were needed to achieve the IC_{50} value in human breast cancer cells grown in 3D (Table 1).

3.4 Glucose consumption and Lactate Dehydrogenase assay

To evaluate whether glucose metabolism of MDA-MB-231 cells is altered in silk constructs, the collected spent media on 1, 4, or 7 days after seeding and glucose concentrations was measured. In 3D silk constructs, the glucose concentration on 7th day was 2.76 ±0.03 mg/mL compared to 2D (7.3±0.08 mg/mL). In 3D silk constructs, 1.3 -fold of increase in LDH activity was observed on 7th day in comparison to 2D. Thus, the glucose consumed and LDH activity was higher in cells grown in 3D constructs than those in 2D (Fig. 4 a-b).

3.5 MMP-9 activity of MDA-MB-231 cells on silk constructs

Matrix metalloproteinase 9 (MMP-9) plays a vital part in the progression of tumor and angiogenesis. To determine the MMP-9 activity SDS-PAGE gelatin zymography was

performed. The spent media of 1, 4, and 7 day of both the constructs (2D and 3D) were assessed for MMP-9 activity (Fig. 5.5). MMP-9 activity was observed in both the 2D and 3D cell cultures. The cells cultured on 3D silk constructs showed higher activity (1.4-fold increase) on 7^{th} day compared to 2D cultures (Fig. 5 a-c). The 3D silk constructs were therefore, used for the experimental drugs studies. The spent media of the cyclosaplin and doxorubicin treated 3D constructs were evaluated for MMP-9 activity. The cyclosaplin and doxorubicin treated MDA-MB-231 cells showed 1.2-1.5 fold decrease in MMP-9 activity in 3D constructs respectively (Fig. 5 d-f).

3.6 Scanning electron microscopy

The scanning electron micrographs revealed the formation of cellular aggregates, distributed homogenously within the 3D silk constructs after a culture period of 7 days in untreated constructs (Fig. 6a). Both cyclosaplin (peptide) (Fig. 6 c-d) and doxorubicin (Fig. 6 e-f) treated (100 µg/mL) constructs exhibited few individual cells that were less in number. Cell shrinkage was also observed in both the treated conditions.

3.7 Live-Dead assay

To study the cell viability of MDA-MB-231 cells after treatment with cyclosaplin (1, 100 µg/mL) and doxorubicin (1, 100 µg/mL), live-dead assay was performed. The number of viable cells decreased in the cyclosaplin and doxorubicin treated cell cultures. The number of live cells was higher in the control silk constructs (Fig. 7a). Some dead cells were also observed in Doxorubicin treated culture (Fig. 7 b-c). The drug induced MDA-MB-231 cells reduced in size displaying unhealthy cell morphometric features (Fig. 7).

3.8 Analysis of cytoskeletal organization

The MDA-MB-231 cells grown on 2D silk constructs were immunostained with actin antibody to visualize the effects of cyclosaplin and doxorubicin on cytoskeletal arrangements. The cyclosaplin and doxorubicin treated cells showed some membrane ruffles and decrease

of cytoskeletal stress fibers (Fig. 8). No such significant changes in cytoskeletal organization were observed in both the cases.

4. Discussion

In this study, 3D breast tumor model was used for culturing MDA-MB-231 cells on *A. mylitta* silk fibroin and screened for efficacy of the experimental anticancer drugs. The objective of this study was to investigate whether efficacy of cyclosaplin and doxorubicin are affected when screened in cells cultured on 3D silk constructs compared to conventional 2D systems prior to future preclinical trials.

For the experimental studies, the *A. mylitta* silk constructs were fabricated [18] to facilitate the attachment and proliferation of human breast cancer cells (MDA-MB-231). The RGD peptide, serves as a recognition site for integrin-mediated cell adhesion present in *A. myllita* fibroin, plays a vital role in cell attachment and proliferation [26]. Scanning electron micrographs revealed the well-interconnected pores ranging from 100 – 300 µm, as well as proliferating MDA-MB-231 cells (Fig. 1). Alamar blue, a redox indicator was used to assess the metabolic function and cellular health of the proliferating cells. The growth of cells was higher on the 4^{th} day but decreased on the 7^{th} day in the 2D constructs. In contrast, the initial growth of cells was slow in 3D silk constructs but increased on the 7^{th} day (Fig. 2). The slow initial growth of cells in 3D culture compared to corresponding 2D was in supportive to earlier reports that describe the difference in cell signaling and cellular functions between 3D and 2D responsible for such phenomena [19]. After initial cell seeding in 3D, the cell adhesion organization develops *in vitro* towards *in-vivo*-like adhesions [3]; that imparts reduced cellular proliferation rate at initial culture period. The cell viability of MDA-MB-231 cells after treatment with cyclosaplin and doxorubicin were investigated using MTT assay (Fig 3 a-b). The 3D silk fibroin constructs showed higher density of cells than that in 2D constructs. For the two experimental drugs cyclosaplin and doxorubicin, the IC_{50} values were

5-6 folds higher than in the 2D monolayer (Table 1). Earlier, anticancer drugs such as doxorubicin, paclitaxel, and tamoxifen have demonstrated 12-23 folds higher IC $_{50}$ value in 3D breast (MCF-7) cancer model compared to 2D systems [27]. Similarly, celexocib, ZD6474, and paclitaxel showed 2-6 folds higher IC_{50} value in 3D silk fibroin tumor model [19]. The higher number of cells could be responsible for increased resistance towards anticancer drugs. The tumor matrix and cells in the tumor might be altering the response of the tumor cells towards treatment of drugs. The complex biological processes involved in the tumor microenvironment defines it part in resolving its phenotype including resistance to drugs [28]. Several researchers have spotlighted the role of 3D cell culture on high resistance to drugs [29-31]. Recently, high-throughput 3D evaluation revealed variation in drug sensitivities between culture models of JIMT1 breast cancer cells (Hongisto et al., 2013). It has long been postulated however that cells grown in 3D matrices can show relative resistance to chemotherapeutic drugs and mimic *in vivo* like conditions, absent in 2D culture systems [34]. Further, glucose metabolism of MDA-MB-231 cells was investigated on 2D and 3D silk constructs. The glucose consumption and LDH activity was significantly high in 3D constructs compared to 2D (Fig 4 a-b). This phenomenon was comparable to earlier reports that describe high glucose consumption and lactic acid production in 3D constructs [18]. Cancer cells ardently use glucose as energy source for and survival in comparison to normal cells [35]. It is observed that cancer cells metabolize glucose into pyruvate producing excess lactate even though there is an adequate supply of oxygen to support mitochondrial respiration [36-37]. The elevated levels of LDH are hallmark of several highly glycolytic tumors that leads to poor prognosis in several cancers [38, 39]. Researchers have shown a positive correlation between lactate levels and tumor burden in cancer patients [38, 39]. Thus, it was postulated that the enhanced levels of LDH and the production of lactic acid by tumor cells might facilitate the escape from immune surveillance [40, 41]. Several researchers have

comparatively evaluated the glucose metabolism in both 2D and 3D tumor models *in vitro* [18, 41]. The MMP-9 activity was higher in 3D cell cultures than 2D suggesting the high proliferative rate, survival, and invasive nature of the breast cancer cells (Fig. 5 a-c). Matrix metalloproteinases (MMPs) have long been connected with cancer-cell invasion and metastasis [11]. MMPs regulate signaling pathways that control cell growth, survival, invasion, inflammation and angiogenesis [43]. The cyclosaplin and doxorubicin treated MDA-MB-231 cells however, showed 1.2-1.5 fold decrease in MMP-9 activity (Fig. 5 d-f). Thus, the decrease in MMP-9 activity suggests the usefulness of cyclosaplin as MMP-9 inhibitor. MMP-9 has been found in large quantities in the cancer tissues and corroborates with the process of tumor cell invasion and metastasis [43, 44]. Recent clinical studies in cancer patients, have implicated that MMP-9 could be a strong and independent marker for aggressive breast cancer [45]. Scanning electron micrographs displayed the cytotoxic effect of cyclosaplin and doxorubicin on MDA-MB-231 cells. The number of cells reduced after treatment with the experimental drugs and showed unusual morphology (Fig. 6). Similarly, live-dead assay showed the detrimental effects of doxorubicin (Fig. 7 b-c) and cyclosaplin (Fig. 7 d-f) on MDA-MB-231 cells, although higher concentrations was a prerequisite to achieve 50% cell death in 3D silk constructs (Fig. 7). The MDA-MB-231 cells treated for 24 h with cyclosaplin and doxorubicin did not apparently modify the MDA-MB-231 actin cytoskeleton but a few membrane ruffles were observed in the cyclosaplin treated cells (Fig. 8). The targeting of actin cytoskeleton is quite old, given its involvement in cell-related processes such as cell division and cell migration [46, 47]. The actin cytoskeleton, therefore, is one of the target points for cancer therapeutics. TR100, a novel class of anti-tropomyosin compounds, is active against a panel of neural crest-derived tumor cell lines in both 2D and 3D cultures with minimum effect on the contractile features of isolated rat adult cardiomyocytes [48]. Previously, the other actin targeting drugs such as cytochalasin D and

jasplakinolide have shown huge potential as antiproliferative agents *in vitro* [49, 50]. Several researchers have reported the different possibilities as to how the 3D microenvironment may influence proliferation, presence or absence of growth factors, cytokines, proteases, or alterations in the composition or structure of ECM proteins [3, 6, 51].

5. Conclusion

The 3D silk fibroin *in vitro* tumor model can affect the proliferation and metabolism of MDA-MB-231 cells compared to 2D cell monolayer. Additionally, it can alter the efficacy of experimental drugs (cyclosaplin and doxorubicin). Overall, the results, throw spotlight on the usefulness of cyclosaplin in cancer therapeutics.

Declaration of interest

The authors declare no conflict of interest.

Acknowledgements

Indian Institute of Technology Kharagpur supported the work and authors would like to acknowledge the Central Research Facility, IIT Kharagpur for providing instrumental support.

References

1. Iivascu, A., Makubbies, K., 2006. Rapid generation of single-tumor spheroids for high throughput cell function and toxicity analysis. Journal of Biomolecular Screening11, 8.

2. Breslin S, O'Driscoll L., 2013. Three-dimensional cell culture: the missing link in drug discovery. Drug Discovery Today 18(5-6), 240-249.

3. Cukierman, E., Roumen P., Kenneth M.Y., 2002. Cell interactions with three-dimensional matrices. Current Opinion in Cell Biology 14,633-639.

4. Inman, J.L., Bissell, J.M., 2010. Apical polarity in three-dimensional culture systems: where to now. Journal of Biology 9, 2.

5. Martin-Belmonte, F., Yu, W., Rodriguez-Fraticelli, A.E., Ewald, A., Werb, Z., Alonso, M.A., 2008. Cell polarity dynamics controls the mechanism of lumen formation in epithelial morphogenesis. Current Biology 18(7), 507-513.

6. Kunz-Schughar, L.A., Freyer, J.P., Hofstaedter, F., Ebner, R., 2004. The use of 3D cultures for high-throughput screening: the multicellular spheroid model. Journal of Bimolecular Screening 9, 273-285.

7. Shin, C.S., Kwak, B., Han, B., Park, K., 2013. Development of an *in vitro* 3D tumor model to study therapeutic efficiency of an anticancer drug. Molecular Pharmaceutics 10(6), 2167-2175.

8. Draoui, N., Feron, O., 2011. Lactate shuttles at a glance: from physiological paradigms to anti-cancer treatments. Disease, Models and Mechanisms 4(6), 727-732.

9. Cairns, R.A., Harris, I.S., Mak, T.W., 2011. Regulation of cancer cell metabolism. Nature Reviews Cancer 11, 85-95.

10. Coussens, L.M., Fingleton, B., Matrisian, L.M., 2002. Matrix metalloproteinase inhibitors and cancer: trials and tribulations. Science 295(5564), 2387-2392.

11. Egeblad, M., Werb, Z., 2002. New functions for the matrix metalloproteinases in cancer progression. Nature Reviews Cancer 2(3), 161-174.

12. Rundhaug, J.E., 2005. Matrix metalloproteinases and angiogenesis. Journal of Cellular and Molecular medicine 9(2), 267-285.

13. Mueller, M.M., Fusenig, N.E., 2004. Friends or foes - bipolar effects of the tumor stroma in cancer. Nature Reviews Cancer 4, 839-849.

14. Lee, J., Cuddihy, M.J., Kotov, N.A., 2008. Three-dimensional cell culture matrices: state of the art. Tissue Engineering Part B Reviews 14(1) 61-86.

15. Vepari, C., Kaplan, D.L., 2007. Silk as a biomaterial. Progress in Polymer Science 32, 991-1007.

16. Subia, B., Kundu SC., 2013. Drug loading and release on tumor cells using silk fibroinalbumin nanoparticles as carriers. Nanotechnology 24(3), 035103.

17. Zhang, X.H., Baughman, C.B., Kaplan, D.L., 2008. *In vitro* evaluation of electrospun silk fibroin scaffolds for vascular cell growth. Biomaterials 29, 2217-2227.

18. Talukdar, S., Mandal, M., Dietmar, W., Hutmacher, P.J., Soekmadji, C., Kundu, S.C.,2011. Engineered silk fibroin protein 3D matrices for in vitro tumor model. Biomaterials 32, 2149-2159.

19. Talukdar, S., Kundu, S.C., 2012. A non-mulberry silk fibroin protein based 3D in vitro tumor model for evaluation of anticancer drug activity. Advanced Functional Materials 22, 4778-4788.

20. Mishra, A., Gauri, S.S., Mukhopadhyay, S.K., Chatterjee, S., Das, S.S., Mandal, S.M.,Dey, S., 2014. Identification and structural characterization of a new pro-apoptotic cyclic octapeptide cyclosaplin from somatic seedling of *Santalum album* L. Peptides 54, 148-158.

21. Kundu, B., Kundu S.C., 2012. Silk sericin/polyacrylamide *in situ* forming hydrogels for dermal reconstruction. Biomaterials 33, 7456-7467.

22. Kundu B., Saha P., Datta K., Kundu S.C., 2013. A silk fibroin based hepatocarcinoma model and the assessment of the drug response in hyaluronan-binding protein 1 over expressed HepG2 cells. Biomaterials 34 (37), 9462-9474

23. Fornari, F.A., Randolph, J.K., Yalowich, J.C., Ritke, M.K., Gewirtz, D.A., 1994. Interference by doxorubicin with DNA unwinding in MCF-7 breast tumor cells. Molecular Pharmacology 45(4), 649-656.

24. Tacar, O., Sriamornsak, P., Das, C.R., 2013. Doxorubicin: an update on anticancer molecular action, toxicity and novel drug delivery systems. Journal of Pharmacology 65,157-170.

25. Corada, M., Mariotti, M., Thurston, G., Smith, K., Kunkel, R., Brockhaus, M., et al., 1999. Vascular endothelial ‐ cadherin is an important determinant of microvascular integrity in vivo. Procedings of National Academy of Sciences of the United States of America 96(17), 9815-9820.

26. Hersel, U., Dahmen, C., Kessler, H., 2003. RGD modified polymers: biomaterials for stimulated cell adhesion and beyond. Biomaterials 24, 4385- 4415.

27. Horning, J.L., Sahoo, S.K., Vijayaraghavalu, S., 2008. 3D tumor model for in vitro evaluation of anticancer drugs. Molecular Pharmacology 5(5), 849-862.

28. Park ,C.C., Bissell, M.J., Hoff, M.H.B., 2000. The influence of the microenvironment on the malignant phenotype. Molecular Medicine Today 6(8), 324-329.

29. Fischbach, C., Chen, R., Polverini, P.J., Mooney, D.J., 2007. Engineering tumors with 3D scaffolds. Nature Methods 4, 855-860.

30. Nirmalanandhan, V.S., Duren, A.P., Vielhauer, H.G., Sittampalam, G.S., 2010. Activity of anticancer agents in a three-dimensional cell culture model. Assay and Drug Development Technologies 8 (5), 581-590.

31. Quanwen, L., Albert, B.C., Mattingly, R.R., 2010. The journal of pharmacology and experimental therapeutics 332(3), 821-828.

32. Starzec, A., Briane, D., Kraemer, N., Kouyoumdjian, J.C., Moretti, J.L., Beaupain R,Oudar, O., 2003. Spatial organization of three-dimensional co-cultures of adriamycin-sensitive and -resistant human breast cancer MCF-7 cells. Biology of the Cell 95(5), 257-264.

33. Hongisto, V., Fey, V., Mpindi, J.P., 2013. High-Throughput 3D Screening Reveals Differences in Drug Sensitivities between Culture Models of JIMT1 Breast Cancer Cells. PlosOne 8 (10), e77232.

34. Weaver, V.M., Lelievre, S., Lakins, J.N., Chrenek, M.A., Jones, J.C., Giancotti, F., Werb, Z., Bissell, M.J., 2002. β4integrin-dependent formation of polarized three-dimensional architecture confers resistance to apoptosis in normal and malignant mammary epithelium. Cancer Cell, 2, 205-216.

35. Salani, B., Rio, A.D., Massollo, M., 2013. Metformin impairs glucose consumption and survival in calu 1 cells by direct inhibition of Hexokinase-II. Scientific Reports 3,2070

36. Warburg O., 1956. On the origin of cancer cells. Science 123, 309-311.

37. Weber, S., Wolf, K., 1977. Two changes of the same nucleotide confer resistance to diuron and antimycin in the mitochondrial cytochrome b gene of *Schizosaccharomyces pombe*. FEBS Letters 237, 31-34.

38. Koukourakis, G., Kelekis, N., Armonis, V., Kouloulias, V., 2009. Brachytherapy for prostate cancer: a systematic review. Advances in Urology, 327945.

39. McCleland, S.E., Marini, C., Ravera, S., Maggi, D., Sambuceti, G., 2013. Replication stress links structural and numerical cancer chromosomal instability. Nature 494,492-496.

40. Walenta, S., Schroeder, T., Mueller-Klieser, W., 2004. Lactate in solid malignant tumors: potential basis of a metabolic classification in clinical oncology. Current Medicinal Chemistry 11, 2195-2204.

41. Walenta, S., Wetterling, M., Lehrke, M., 2000. High lactate levels predict likelihood of metastases, tumor recurrence, and restricted patient survival in human cervical cancers. Cancer Research 60, 916-921.

42. Chitcholtan, K., Sykes, P.H., Evans, J.J., 2012. The resistance of intracellular mediators to doxorubicin and cisplatin are distinct in 3D and 2D endometrial cancer. Translational Medicine 10, 38.

43. Bauvois, B., 2012. New facets of matrix metalloproteinases MMP-2 and MMP-9 as cell surface transducers: Outside-in signaling and relationship to tumor progression. Biochimica et Biophysica Acta 1825 29 -36.

44. Decock, J., Hendrickx, W., Vanleeuw, U., Van B.V., Van H.S., Christiaens, M.R., Ye,S., Paridaens, R., 2008. Plasma MMP1 and MMP8 expression in breast cancer: protective role of MMP8 against lymph node metastasis. BMC Cancer 20, 8-77.

45. Patel, S., Sumitra, G., Koner, B.C., Saxena, A., 2011. Role of serum matrix metalloproteinase 2 and 9 to predict breast cancer progression. Clinical Biochemistry 44, 869-872.

46. Hall, A., 2009. The cytoskeleton and cancer. Cancer Metastasis Reviews 28, 5-14.

47. Yamaguchi, H., Condeelis, J., 2007. Regulation of the actin cytoskeleton in cancer cell migration and invasion. Biochimica et Biophysica Acta 1773, 642- 652.

48. Stehn, J.R., Nikolas, K.H., Teresa, B., 2013. A Novel class of anticancer compounds targets the actin cytoskeleton in tumor cells. Cancer Research 73, 5169-5182.

49. Bousquet, P.F., Paulsen, L.A., Fondy, C., Lipski, K.M., Loucy, K.J., Fondy, T.P., 1990. Effects of cytochalasin B in culture and in vivo on murine Madison 109 lung carcinoma and on B16 melanoma. Cancer Research 50, 1431-1439.

50. Senderowicz, M.J., 1995. Jasplakinolide's Inhibition of the Growth of Prostate Carcinoma cells *In Vitro* with disruption of the actin cytoskeleton. Journal of the National Cancer Institute 87 (1), 46-51.

51. Barkan, D., Justin L.S., Kamaraju A.K., Mark J., Cho E.C., Lockett S., Khanna C., Chambers A.F., Green J.E., 2008. Inhibition of Metastatic Outgrowth from Single Dormant tumor Cells by targeting the Cytoskeleton. Cancer Research 68, 6241-6250.

Table 1 Chemotherapeutic studies of cyclosaplin and doxorubicin

Drug	IC $_{50}$ (µg/mL)		Fold change in
	2D monolayer	3D model	IC_{50}
Cyclosaplin	16.8 6 ± 0.09	89.27 ± 0.2	5.3
Doxorubicin	2.8 ± 0.06	16.44 ± 0.1	5.9

Figure Legends

Fig. 1 Fabrication of silk 2D and 3D silk constructs. a) - c) A.mylitta silk fibroin 2D construct seeded with MDA-MB-231 cells for 1st day, 3rd day and 5th day. d) *A.mylitta* silk fibroin constructs. e) Scanning electron micrograph of *A.myliita* construct w/o cells (Scale bar = 100 µm). f) *A. mylitta* fibroin construct seeded with MDA-MB-231 cells for 7 days (Scale bar = 50 µm).

Fig. 2 The cell proliferation of MDA-MB-231 cells grown on 2D and 3D silk fibroin constructs over a culture period of 7 days. The highest cell growth was observed on 4th day in the 2D constructs. The proliferation of cells in 3D, increased over time and is higher than 2D on 7th day. The error bars indicate ± SD (standard deviation for n = 3)

Fig. 3 Viability of MDA-MB-231 cells treated with cyclosaplin and doxorubicin. The MDA-MB-231 cells were grown for 7 days before treatment. a) cyclosaplin (peptide) treated MDA-MB-231 cells on silk constructs. b) doxorubicin (anticancer drug) treated MDA-MB-231 cells on silk constructs. The error bars indicate ± SD (standard deviation for n = 3).

Fig. 4 Glucose metabolic studies of MDA-MB-231 cells cultured on 2D and 3D silk constructs a) glucose concentration (mg/ml) and b) LDH activity (U/mL) in the spent media of cells grown on 2D and 3D constructs. The data is denoted as mean ± SD (n = 3, $P < 0.01$, $P < 0.05$)

Fig. 5 The zymograph of spent media from MDA-MB-231 cells cultured on constructs. a) Lane 1- Lane 3: 2D *A. mylitta* coated silk constructs (Day 1, Day4, Day 7) Lane 4 - Lane 6: 3D *A. mylitta* silk fibroin scaffolds, Lane 7: Collagenase (Positive control), Bands were analyzed using Image J software and represented as b) mean area and c) mean intensity (arbitrary units). Zymograph of drug treated spent media from MDA-MB-231 cells grown on 3D constructs. d) Lane 1-Lane 2: doxorubicin treated *A.mylitta* silk fibroin constructs, Lane 3 – Lane 4: cyclosaplin treated *A.mylitta* silk fibroin constructs, Lane 5: control, and Lane 6: Collagenase (Positive control), Bands were analyzed using Image J software and represented as e) mean area and f) mean intensity (arbitrary units).

Fig. 6 Cell loaded 3D silk constructs displaying treated and untreated conditions. a) –b) MDA-MB-231 cells loaded silk fibroin construct without treatment. c) – d) Peptide treated (cyclosaplin) MDA-MB-231 cells on *A.mylitta* silk fibroin. e) – f) doxorubicin treated MDA-MB-231 cells on *A. mylitta* silk fibroin. Scale bar = 50 and 10 µm.

Fig. 7 Live-dead stained confocal micrographs showing morphology of MDA-MB-231 cells. a) Untreated MDA-MB-231 cells b) doxorubicin treated cells (1µg/mL) c) doxorubicin treated cells (100 µg/mL) d-f) cyclosaplin treated cells (1-100 µg/mL). Scale bar = 200 µm

Fig. 8 Cytoskeletal organization of MDA-MB-231 cells by actin immunostaining. a)-d) MDA-MB-231 cells without treatment. b-e) MDA-MB-231 cells treated with doxorubicin. c-f) cyclosaplin treated MDA-MB-231 cells (Scale bar = 50 µm and 20 µm).

Figure 1

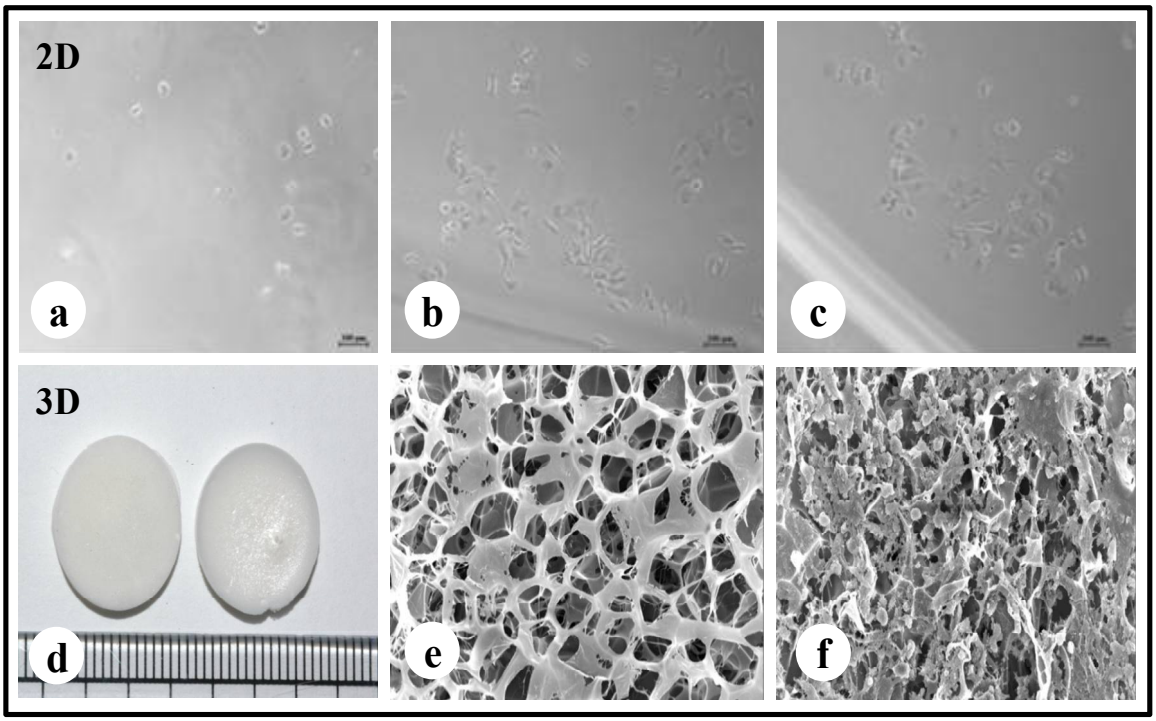

Figure 2

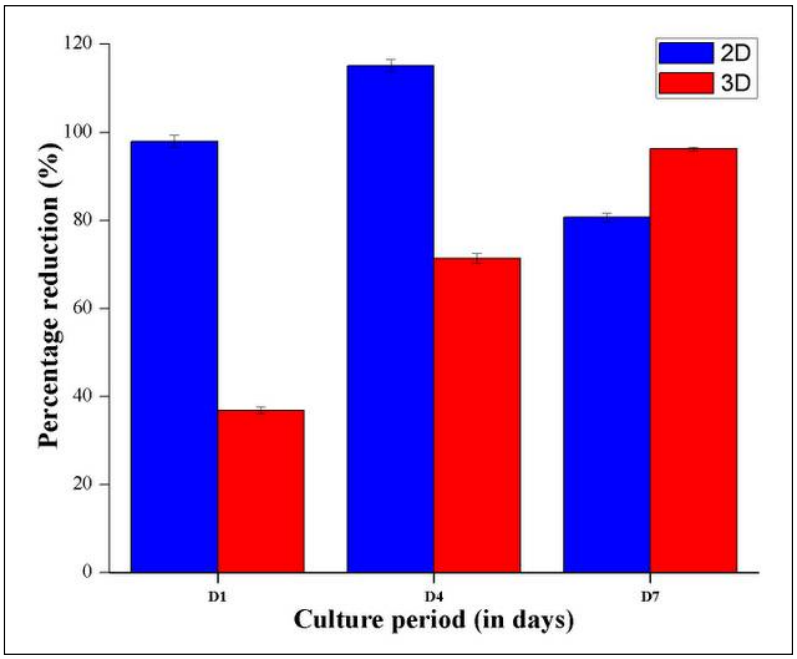

Preprints (www.preprints.org) | NOT PEER-REVIEWED | Posted: 29 January 2019 doi:10.20944/preprints201901.0283.v1

Peer-reviewed version available at Biomolecules 2019, 9, 123; doi:10.3390/biom9040123

Figure 3

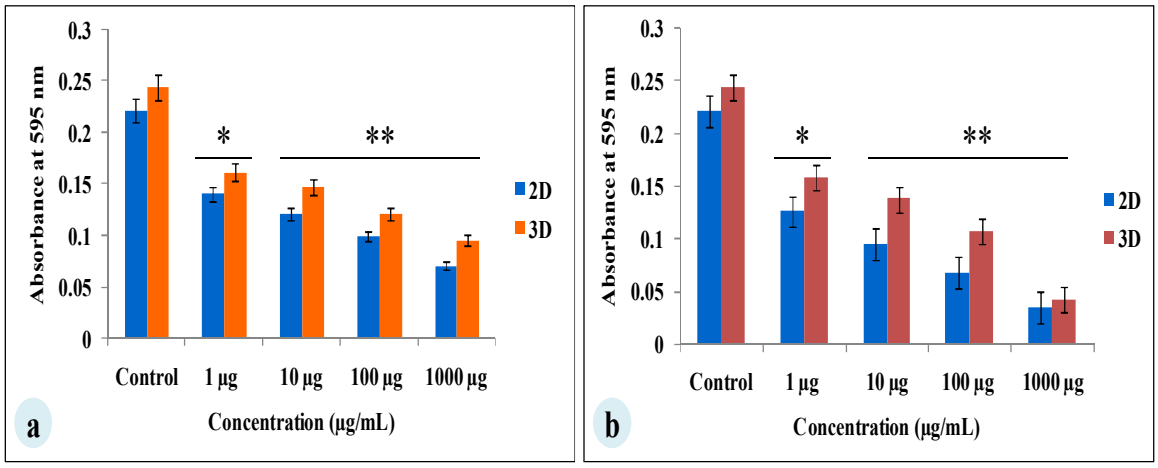

Figure 4

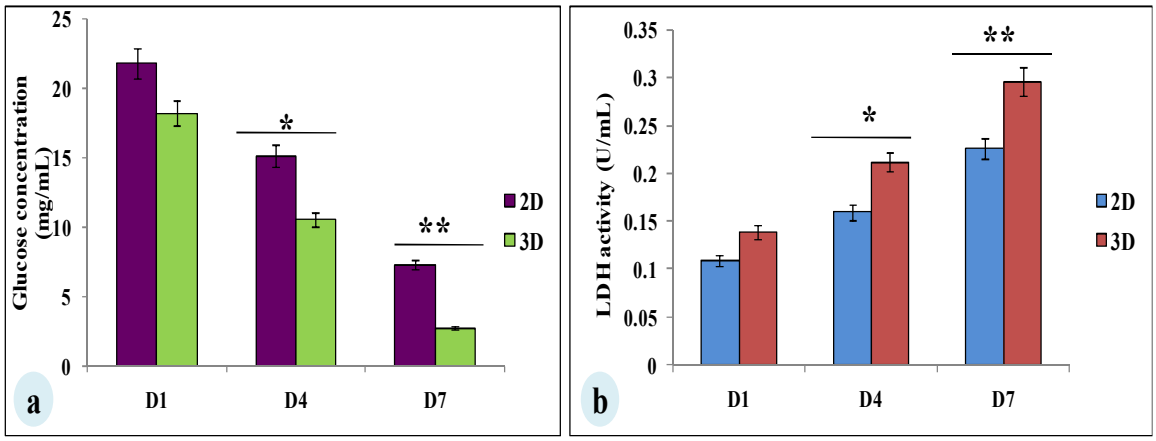

Preprints (www.preprints.org) | NOT PEER-REVIEWED | Posted: 29 January 2019 doi:10.20944/preprints201901.0283.v1

Peer-reviewed version available at Biomolecules 2019, 9, 123; doi:10.3390/biom9040123

Figure 5

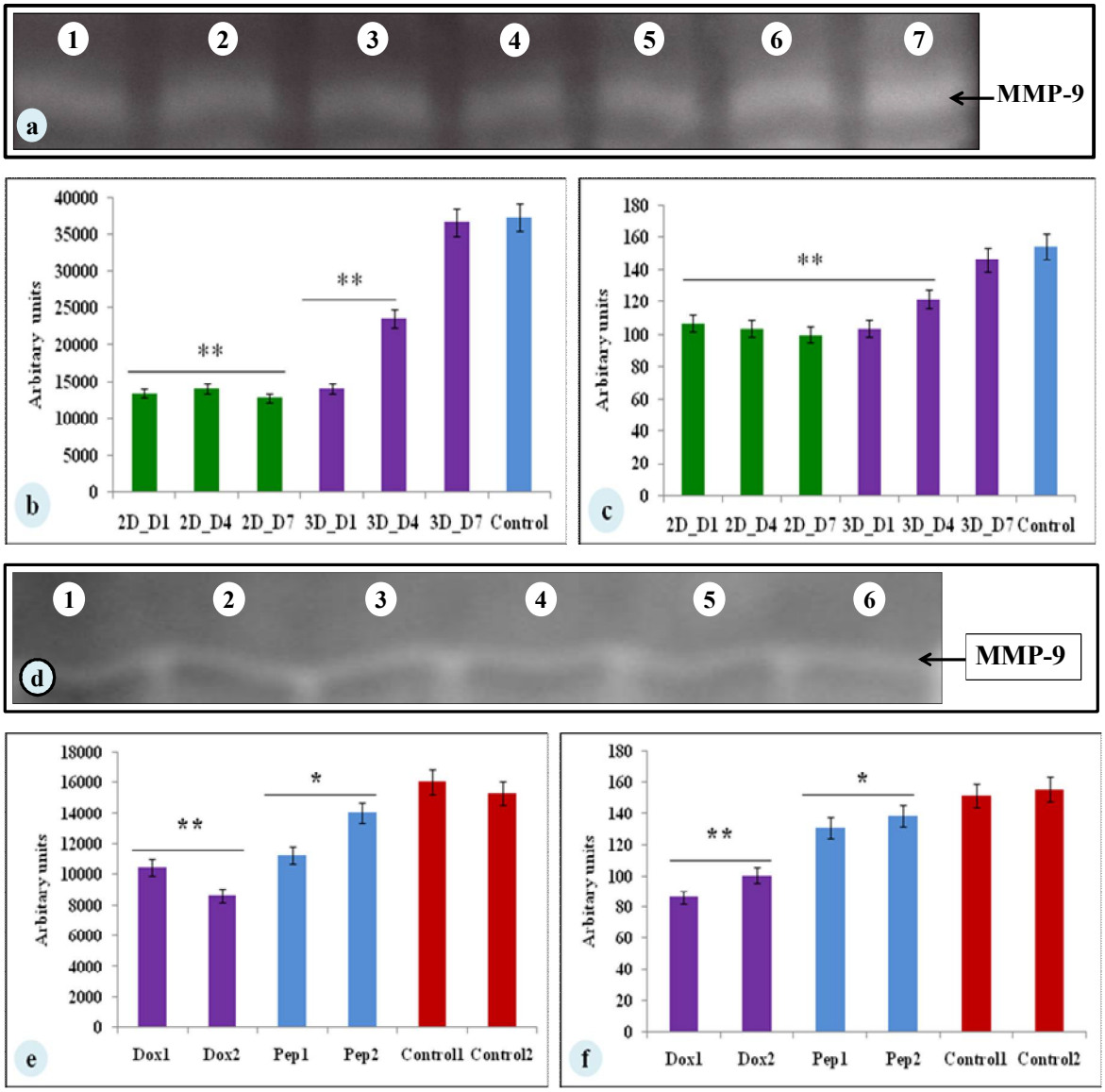

Figure 6

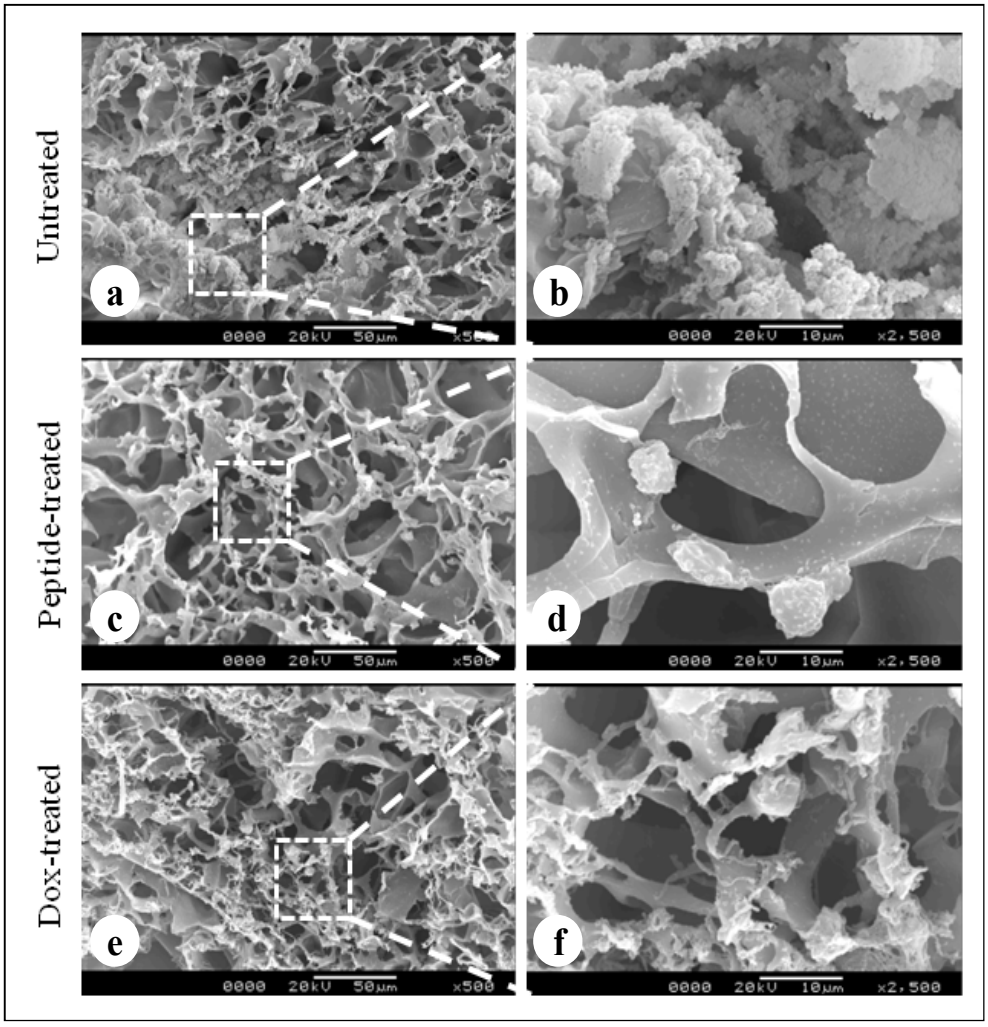

Figure 7

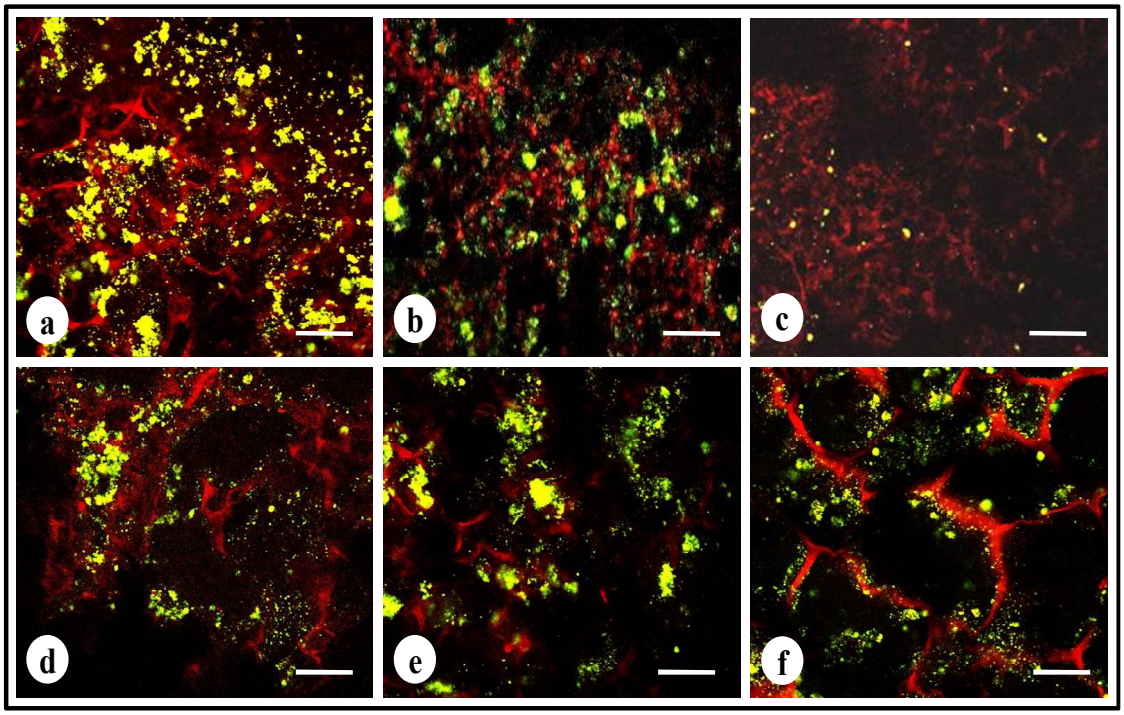

Figure 8